INSTITUTE OF PHYSICS PUBLISHING and INTERNATIONAL ATOMIC ENERGY AGENCY NUCLEAR FUSION

Nucl. Fusion **44** (2004) 303–311 PII: S0029-5515(04)73454-7

Modelling of PPCD in the reversed field pinch RFX by the transport code RITM

G. Telesca[1] **and M.Z. Tokar**[2]

[1] Laboratory for Plasma Physics, Association EURATOM-Belgian State, Koninklijke, Militaire School-Ecole Royale Militaire, Renaissancelaan, 30, avenue de la Renaissance, B-1000 Brussels, Belgium[a]

[2] Institut fuer Plasmaphysik, Forschungszentrum Juelich GmbH, EURATOM Association, D-52425 Juelich, Germany[a]

Received 2 January 2003, accepted for publication 9 December 2003
Published 16 January 2004
Online at stacks.iop.org/NF/44/303 (DOI: 10.1088/0029-5515/44/2/012)

Abstract

The modifications in plasma parameters and heating power under conditions of pulsed poloidal current drive (PPCD) in Reversed Field eXperiment (RFX) are modelled by the one-dimensional transport code RITM (Radiation from Impurities in Transport Model). Several channels for the PPCD effects on plasma confinement are taken into account: dissipation of externally driven poloidal currents, reduction in the electric field induced by the dynamo and decrease in magnetic fluctuations. It is demonstrated that the external currents are dissipated at the plasma edge and they cannot, alone, lead to any change in the temperature profile. The reduction in the dynamo electric field results in central peaking of the current and Ohmic power densities, accompanied, however, by a very modest rise in the central temperature. By taking into account the decrease in the level of magnetic fluctuations (predicted for PPCD conditions by non-linear MHD simulations) and the corresponding reduction of transport in the stochastic magnetic field, RITM reproduces, in agreement with experiments, a significant increase in the central temperature and a reduction in the loop voltage.

PACS numbers: 52.55.Lf, 52.55.Wq, 52.65.Kj

1. Introduction

Pulsed poloidal current drive (PPCD) induced by a transient change in the edge toroidal magnetic field affects significantly the magnetic and confinement properties of the reversed field pinch (RFP). Common features in the Madison Symmetric Torus [1] and in Reversed Field eXperiment (RFX) (major radius, 2 m; minor radius, 0.46 m) [2, 3] are the high current density on the plasma axis, the lower magnetic fluctuation level, the increase in the stored plasma energy and a significant reduction in the loop voltage. The reaction of the plasma to the externally driven currents is generally attributed to a reduction in the self-organizing dynamo electric field [4], which is necessary to maintain a force-free equilibrium in the RFP configuration, counteracting the resistive diffusion of the magnetic field [5]. Fluctuations of the plasma velocity and magnetic field that generate the dynamo field lead, however, to large particle and energy losses, which are the main impediment for a better confinement in RFPs. Therefore, the possibility of reaching a RFP equilibrium with a reduced necessity for the dynamo field, and consequently with a reduced level of stochasticity and losses, renders the study of PPCD plasmas of crucial relevance for any future development of RFP.

[a] Partners in the Trilateral Euregio Cluster.

The foregoing underlines a fundamental role of non-linear magnetohydrodynamics (MHD) simulations (see [6, 7]) for the analysis of RFP plasmas and, in particular, of the effects from PPCD. Such simulations require as an input the profiles of plasma parameters, e.g. the plasma temperature, density, effective ion charge, etc. In an ideal case, modelling of these profiles should be done self-consistently with MHD simulations, however, a significant difference in the characteristic times of MHD and transport processes allows us in the first approximation to simulate them independently. In this paper we present the results of our transport modelling by the one-dimensional transport code RITM (Radiation from Impurities in Transport Model) [8] of the PPCD effect on the plasma profiles. In order to get a qualitative understanding, we have modelled separately and then also simultaneously the influence of (i) externally driven poloidal currents, (ii) the reduction in dynamo electric field leading to the peaking of the input power and current density profiles and (iii) the decrease in transport coefficients due to reduction in magnetic fluctuations. The changes in turbulence characteristics with PPCD and their dependence on plasma parameters are taken as prescribed from the results of MHD simulations and experimental data. Our intention is to model a typical PPCD on RFX and the related physical mechanisms, and we did not make any effort to model

a single special experimental situation, which may change, depending upon many factors (the level and waveform of the field from external coils, plasma–wall interaction, the presence of the locked mode, the plasma purity and so on).

In section 2, the version of the RITM code adapted to model RFP standard discharges is described. In section 3, the equations required for modelling PPCD conditions and describing the evolution of the external current and the modification of the magnetic configuration and of the heating power density are derived. The results of PPCD modelling are presented in section 4, and conclusions are drawn in section 5.

2. RITM code for standard RFX discharges

2.1. General structure of the code

The predictive transport code RITM [8] has been originally developed for modelling of tokamak plasmas (including Tore Supra plasmas with a stochastic edge layer [9]). Later, it has been adapted to model particle, heat and impurity transport in the fully stochastic field of RFPs, and the basic features of this code version as well as some relevant results are given in [10, 11].

RITM is a one-dimensional code that solves time dependent continuity equations for neutral and charged particles of background plasma and impurities and energy balance equations for electrons and ions. These equations are averaged over circular magnetic surfaces with coordinates (r, θ, z), which simulate the torus with $z = R\phi$. As an output, RITM provides the self-consistent time evolution of the radial profiles of the density of neutral and charged particles (background and impurities) and temperatures of electrons and ions, $T_{\mathrm{e,i}}$.

The continuity equation for electrons takes into account the transport channels through radial diffusion and convection and sources from ionization of recycling neutrals and impurities. The following particularly important components of neutrals are taken into account: molecules desorbed from the machine walls, atoms produced by reflection of plasma ions, Frank–Condon atoms generated by dissociation of molecules, and hot atoms created by charge exchange with plasma ions. A rather sophisticated description of the particle recycling allowed us to reproduce the variation of H_α signals and particle confinement time with the plasma parameters in the tokamak TEXTOR [8]. Impurity ions are described in a non-corona approximation by taking into account both transport and elementary processes like ionization, recombination and charge exchange with hydrogen neutrals. This provides the density of radiation losses. These losses are included into the equation for the energy balance of electrons together with the losses on ionization of recycling neutrals, energy exchange with ions in Coulomb collisions and energy source from Ohmic heating, $Q_{\mathrm{OH}} = \eta j^2$. The Spitzer resistivity, η, is computed by using the electron temperature and ion effective charge calculated from the electron and impurity densities.

The radial profiles of the magnetic field and current density components are computed according to the modification of the Taylor's relaxation theory for a force-free equilibrium [5], the so-called μ and p model, in which the value $\mu = jB/B^2$ is an assigned function of the radius, and use is made of the radial component of the plasma equilibrium equation, $\nabla p = (1/c)\,[j \times B]$. The parallel current density profile is calculated assuming $\mu = (2\theta_0/a)\,f$, $f = 1 - (r/a)^\alpha$, with a being the plasma minor radius, and θ_0 and α are given parameters, which characterize the on-axis current density and broadness of the current profile, respectively. The perpendicular current is computed using the pressure profile. For typical RFX discharges without PPCD, $\theta_0 = 1.4$ and $\alpha = 8$.

The boundary conditions at the LCFS are given by the e-folding lengths of density and temperature, λ_{n} and $\lambda_{T_{\mathrm{e,i}}}$, respectively. These are taken from the measurements in the scrape-off layer, and typically $\lambda_{\mathrm{n}} = 0.5\,\mathrm{cm}$, $\lambda_{T_{\mathrm{e}}} = 4\,\mathrm{cm}$, $\lambda_{T_{\mathrm{i}}} = 8\,\mathrm{cm}$. During the PPCD phase, the e-folding lengths decrease to values of 0.3 cm, 2 cm and 4 cm, respectively.

2.2. Transport coefficients

The plasma transport characteristics in a stochastic magnetic field of RFPs are essentially determined by the diffusivity of field lines, D_{FL}. In a quasi-linear approximation [12],

$$D_{\mathrm{FL}} = \left(\frac{\delta b_{\mathrm{r}}}{B}\right)^2 L_{\parallel}, \tag{1}$$

where δb_{r} is the radial component of the magnetic fluctuations and $L_{\parallel}$ is their parallel correlation length, being of the order of a for RFX plasmas [13]. According to experimental measurements [14] and the results of non-linear MHD simulations [6], the magnitude of $\delta b_{\mathrm{r}}/B$ depends on the plasma parameters through the Lundquist number, S, the ratio of characteristic resistive and Alfvén times. Therefore, the transport coefficients also depend on S. In particular, the heat diffusivity in the plasma core of RFX decreases with S roughly as $S^{-0.7}$ [15]. In order to satisfy this, it was assumed that $\delta b_{\mathrm{r}}/B = kS^{-0.35}$, with the factor k chosen to reproduce $\delta b_{\mathrm{r}}/B$ of 10^{-2} as measured under standard RFX conditions. For PPCD conditions, k is reduced by a factor of 0.7, corresponding to the reduction in the global energy of the magnetic fluctuations, $E^{\mathrm{M}} \sim b_{\mathrm{r}}^2$, by a factor of 2, as found in MHD numerical simulations [7].

The effective heat conductivity in a stochastic magnetic field is computed according to the formulae of [16], modified in order to describe both collision-free and collision dominated transport regimes in an integrated way

$$\chi_{\mathrm{e,i}} = D_{\mathrm{FL}} v_{\mathrm{th\ e,i}} \times \min(1, \lambda_{\mathrm{c}}/\lambda_{\mathrm{K}}). \tag{2}$$

Here, $v_{\mathrm{th\ e,i}}$ are the thermal velocities of electrons and ions, respectively, λ_{c} the mean free path of particles between Coulomb collisions and λ_{K} the Kolmogorov length. The collision-free situation is typical for the central plasma, but at the plasma edge, collisions dominate the transport. The latter explains the experimentally observed drastic decrease in $\chi_{\mathrm{e,i}}$ when approaching the LCFS (see [3]). For λ_{K}, we have used a value of $40a \approx 18\,\mathrm{m}$, in agreement with the estimate given in [17] based on typical RFP spectra of magnetic field perturbations.

The particle flux is composed of diffusive and convective contributions: $\Gamma = -D_{\mathrm{eff}} \times \mathrm{d}n/\mathrm{d}r + V_{\mathrm{eff}} \times n$. The former one is due to thermal motion along the stochastic field lines with

the effective perpendicular diffusivity calculated according to the formula [18]

$$D_{\rm eff} = c_{\rm s} D_{\rm FL}, \tag{3a}$$

where $c_{\rm s} = [(T_{\rm e} + T_{\rm i})/m_{\rm i}]^{1/2}$ is the sound speed. Following [19], two components are included in the effective convective velocity

$$V_{\rm eff} = -D_{\rm eff} \frac{{\rm d}\ln\sqrt{T_{\rm e}}}{{\rm d}r} + V_{E\times B}. \tag{3b}$$

The former one is due to the asymmetry in the velocity distribution function of charged particles caused by the temperature gradient [20] and is directed outwards (anti-pinch) for a normally peaked $T_{\rm e}$ profile. The latter one, which is caused by the drift in the electric field, is inward directed and it was assumed on the basis of analysis in [19] to increase linearly with the minor radius: $V_{E\times B} = -(r/a) \times 7\,{\rm m\,s^{-1}}$.

Transport of impurities in a stochastic field is a complex matter (see, e.g. [21, 22]), which is outside the scope of this work. We have used a simple model with the impurity diffusivity equal to that of the main particles and a convective inward directed velocity, $V_{\rm imp} = V_{E\times B}$. In spite of its simplicity, this model allows us to reproduce satisfactorily such important experimental data as the radiated power density and ion effective charge, $Z_{\rm eff}$ [10].

3. Amendments in RITM for modelling of PPCD

3.1. Effect of reduction in the electric field induced by dynamo

According to non-linear MHD modelling [6, 7] and experiments [14], PPCD leads to a significant reduction in the energy of plasma fluctuations. In addition to the decrease in transport coefficients, this results in a decrease in the dynamo electric field, $E_{\rm D}$. As demonstrated in [23], the power density due to this component changes its sign from negative to positive by going from the plasma axis to the edge so that the total power is nearly zero. Thus, if the contribution from $E_{\rm D}$ is reduced, one should expect more centrally peaked power and current density profiles, as was found in MHD modelling [7]. Henceforth, it will be assumed by following [7] that during the PPCD phase $E_{\rm D}$ is reduced by a factor $\xi \approx 0.5$.

We proceed from the Ohmic law for a force-free equilibrium with zero plasma mass velocity [23],

$$\vec{E}_{\rm i} + \vec{E}_{\rm D} = \eta \vec{j}, \tag{4}$$

where the induced electric field has only a toroidal component, i.e. $\vec{E}_{\rm i} = E_{{\rm i}\varphi}\vec{e}_\varphi$. The variation of $E_{{\rm i}\varphi}$ over the plasma minor radius can be estimated from the Maxwell equation, $\nabla \times E = -(1/c)(\partial B/\partial t)$, as $\Delta E_{{\rm i}\varphi} = (1/c\tau)\int_0^a \Delta B_\vartheta\,{\rm d}r$, where ΔB_ϑ is the change in the poloidal magnetic field during a non-stationary process with a characteristic time τ. For PPCD, one can estimate from figure 7(*b*) $\Delta B_\vartheta \approx 0.05 B_\vartheta(a) \approx 0.015$–$0.02$ T averaged over the plasma minor radius. Thus, for short transient phases with a τ of 1 ms, one obtains a $\Delta E_{{\rm i}\varphi}$ comparable with a typical $E_{{\rm i}\varphi}$ in RFX plasmas of $3\,{\rm V\,m^{-1}}$. For a more realistic τ of a total PPCD phase duration in RFX of 4–5 ms [7], $\Delta E_{{\rm i}\varphi}$ is smaller by a factor of 4–5 than $E_{{\rm i}\varphi}$. Henceforth, we neglect $\Delta E_{{\rm i}\varphi}$ and assume $E_{{\rm i}\varphi}(r) = {\rm const}$.

By integrating the scalar product of equation (4) with $\vec{j}$ over the plasma minor radius and by taking into account that the net dynamo power, $\int \vec{E}_{\rm D}\cdot\vec{j}2\pi r\,{\rm d}r$, is close to zero (see [23]), we find a relation for $E_{{\rm i}\varphi}$,

$$E_{{\rm i}\varphi} I_\varphi \approx \int_0^a Q^0_{\rm OH}\, 2\pi r\,{\rm d}r.$$

Here, I_φ is the total toroidal plasma current and $Q^0_{\rm OH} = \eta_\parallel j_\parallel^2$ is the Ohmic power density before PPCD, with $\eta_\parallel$ being Spitzer's parallel plasma resistivity. Since the ratio of perpendicular to parallel current is of the order of $\beta_{\rm pol}$ (= a few per cent), the contribution of perpendicular diamagnetic currents to $Q^0_{\rm OH}$ is neglected. From the scalar product of equation (4) with $\vec{B}$, we find now the parallel component of the dynamo induced field

$$E_{{\rm D}\parallel} = \eta_\parallel j_\parallel - \frac{B_\varphi}{B I_\varphi}\int_0^a Q^0_{\rm OH}\, 2\pi r\,{\rm d}r,$$

where $B = |\vec{B}|$.

The dynamo induced field is reduced during PPCD by a factor $\xi < 1$. Thus, the total parallel electric field and the power density are modified as

$$E_\parallel = E_{{\rm i}\parallel} + \xi E_{{\rm D}\parallel} = (1-\xi)\frac{B_\varphi}{B I_\varphi}\int_0^a Q^0_{\rm OH} 2\pi r'\,{\rm d}r' + \xi\eta j_\parallel$$

and

$$Q^{\rm dyn}_{\rm OH} = E_\parallel j_\parallel = (1-\xi)\frac{B_\varphi}{B I_\varphi} j_\parallel \int_0^a Q^0_{\rm OH} 2\pi r'\,{\rm d}r' + \xi Q^0_{\rm OH}.$$

With the prescribed relation between parallel current density and magnetic field, $j_\parallel = (c/4\pi)(2\theta_0/a) f(r) B$, and by setting $b_\varphi = (B_\varphi/B_\vartheta(a)) = B_\varphi(ca/2I_\varphi)$ and $\rho = (r/a)$, one finally has

$$Q^{\rm dyn}_{\rm OH}(\rho) = 2(1-\xi)\theta_0 f(\rho) b_\varphi \int_0^1 Q^0_{\rm OH}(\rho')\rho'\,{\rm d}\rho' + \xi Q^0_{\rm OH}(\rho). \tag{5}$$

Here, θ_0, $f(\rho)$ and $Q^0_{\rm OH}$ refer to the phase before the application of PPCD. The current density profile corresponding to the power density given by equation (5) is calculated according to the relation

$$j^{\rm dyn}_\parallel = \frac{cB}{2\pi a}\theta_0 f \sqrt{\frac{Q^{\rm dyn}_{\rm OH}}{Q^0_{\rm OH}}}. \tag{6}$$

The magnetic field components corresponding to the new force-free equilibrium configuration with $j^{\rm dyn}_\parallel$ are determined in appendix A. Finally, one can find the new $\mu_{\rm dyn} = (4\pi/c)(j^{\rm dyn}_\parallel/B)$. An approximation of the $\mu_{\rm dyn}$ radial profile by the formula $\mu = (2\theta_0/a)\,[1 - (r/a)^\alpha]$ provides typically $\theta_0 \approx 1.5$ and $\alpha \approx 6$ during the PPCD phase (see figure 7(*a*)).

3.2. Effect of externally driven currents

In addition to the reduction in the dynamo electric field, the current distribution in the plasma is changed due to the penetration of externally driven currents. By using the Maxwell equation,

$$\frac{{\rm d}B_{\phi,{\rm ext}}}{{\rm d}r} = -\frac{4\pi}{c} j_{\rm ext}, \tag{7}$$

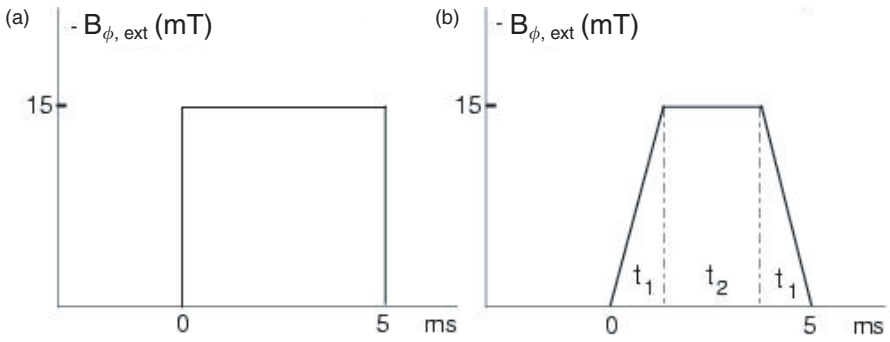

Figure 1. Wave functions of the externally applied field, $B_{\phi,\mathrm{ext}}$.

these currents can be related to the toroidal field component produced by the PPCD coils, $B_{\phi,\mathrm{ext}}$. The time variation of $B_{\phi,\mathrm{ext}}$ at the plasma boundary, $B_{\phi,\mathrm{ext}}(a)$, is prescribed. Assuming zero mass velocity, the penetration of $B_{\phi,\mathrm{ext}}$ into the plasma is described by the equation

$$\frac{4\pi}{c^2}\frac{\partial B_{\phi,\mathrm{ext}}}{\partial t} = \frac{1}{r}\frac{\partial}{\partial r}\left(\eta r \frac{\partial B_{\phi,\mathrm{ext}}}{\partial r}\right). \tag{8}$$

By knowing j_{ext}, one can calculate the total parallel current density, $j_{\parallel}^{\mathrm{ext+dyn}}$ (see appendix B). The total heating power density is given by the relation

$$Q_{\mathrm{OH}}^{\mathrm{ext+dyn}} = \eta (j_{\parallel}^{\mathrm{ext+dyn}})^2. \tag{9}$$

4. Results

In this section, the results of simulations of RFX discharges with $I_{\mathrm{p}} = 850\,\mathrm{kA}$ and $n_{\mathrm{e}} = 5 \times 10^{19}\,\mathrm{m}^{-3}$ are presented. Since the growth rate of $B_{\phi,\mathrm{ext}}(a)$ affects the level of the computed transient increase in the Ohmic power, we consider two shapes of the time trace of $B_{\phi,\mathrm{ext}}(a)$, shown in figure 1. The level of the transient increase in the power, computed for different $B_{\phi,\mathrm{ext}}(a)$ waveforms, is compared in secttion 4.4 with the level of the power experimentally determined using the measured current and voltage on external coils during PPCD. The flat top of $B_{\phi,\mathrm{ext}}(a) = -0.04 B_{\theta}(a) = -15\,\mathrm{mT}$ corresponds to a typical current in the toroidal PPCD coils of RFX of 1 kA per winding. The results of calculations with the step-like time dependence of $B_{\phi,\mathrm{ext}}(a)$ shown in figure 1(a) are presented in 4.1–4.3. Section 4.4 is devoted to consideration of a PPCD pulse with a more realistic trapezoidal form (figure 1(b)).

4.1. Penetration of externally driven currents

In order to analyse the relative importance of different effects from PPCD, they were included into calculations step by step. First, we consider the case when only the influence of external currents on the heating power is taken into account while the effect on turbulence is disregarded by keeping $\xi = 1$ and without reducing the factor k (see, section 2.2) during the whole discharge. Figure 2 displays the radial profiles of j_{ext} for different times. Due to the relatively high plasma resistivity, j_{ext} is nearly completely dissipated before it penetrates to half the minor radius.

In the main part of the plasma, the change in the poloidal plasma current caused by the externally driven currents is very small. This can be seen in figure 3, where j_{ext} is shown at $t = 0.1$ and 5 ms together with the equilibrium poloidal currents, j_{ϑ}, at $t = -2$ ms. Conversely, at the plasma edge, j_{ext} even exceeds j_{ϑ}. Therefore, j_{ext} can noticeably contribute to the total Ohmic power due to the low temperature and high resistivity at the plasma edge. This is confirmed by the time evolution of P_{OH} shown in figure 4: at $t = 0.1$ ms, the total power is about 34 MW, i.e. 7 MW larger than the value of 27 MW computed for the pre-PPCD phase. This variation in P_{OH} found under the (unrealistic) instantaneous increase in $B_{\phi,\mathrm{ext}}(a)$ gives the upper limit for the rise in P_{OH}.

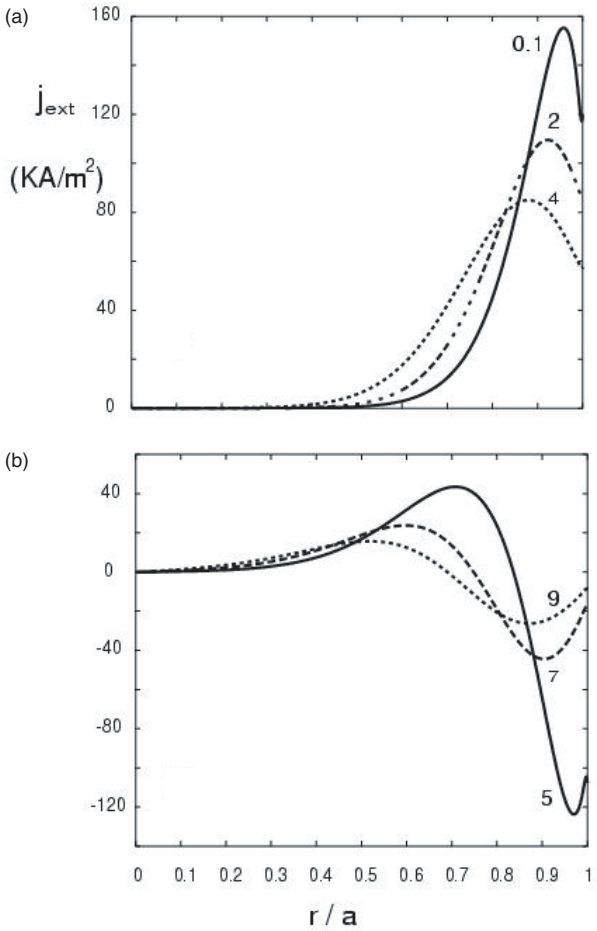

Figure 2. Radial profile of the externally driven poloidal current, j_{ext}, at $t = 0.1$, 2, 4 ms (a) and $t = 5$, 7, 9 ms (b).

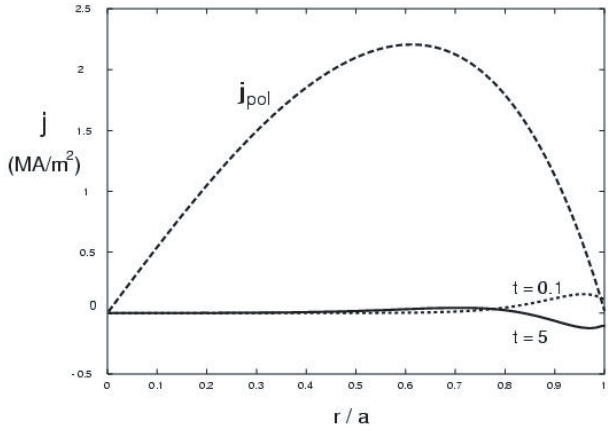

Figure 3. Radial profiles of the externally driven poloidal current, $j_{\rm ext}$, at $t = 0.1$, 5 ms and of the equilibrium poloidal current, $j_{\rm pol}$, at $t = -2$ ms.

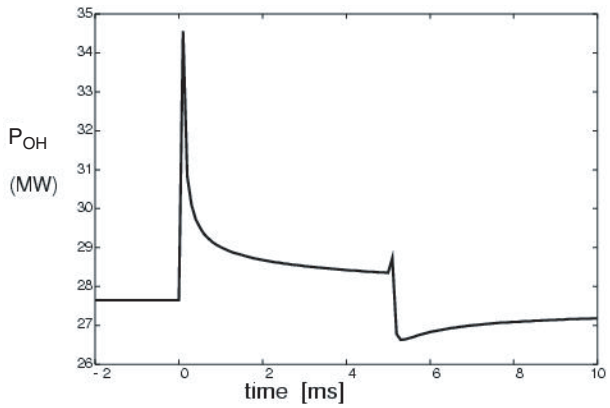

Figure 4. Time trace of the total power in the presence of $j_{\rm ext}$.

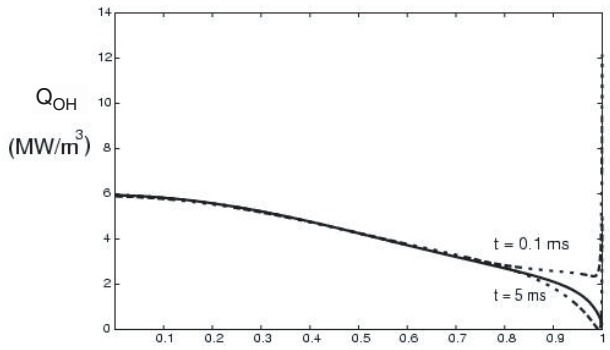

Figure 5. Power density profiles calculated at $t = -2$ (——), 0.1 and 5 ms in the case when only the dissipation of externally induced currents is taken into account.

The contribution from $j_{\rm ext}$ to the heating power is concentrated at the very edge (see power density profiles in figure 5) and is lost very fast from the plasma. Therefore, the electron temperature profile remains unchanged with respect to the pre-PPCD phase. The radiated power density and $Z_{\rm eff}$ are practically unaffected by the external drive. The reversal parameter, F, the ratio of the toroidal magnetic field at the plasma boundary to its averaged value, becomes more negative, decreasing from the reference value $F = -0.1$ to -0.16, and stays approximately constant for 5 ms. The pinch parameter

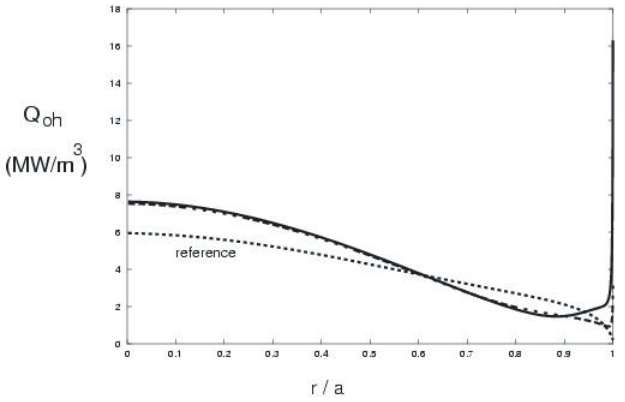

Figure 6. Power density profiles computed at $t = -2$ ms (reference), at $t = 0.2$ (——) and 1 ms (- - - -) in the case when in addition to $j_{\rm ext}$ the reduction in dynamo field is taken into account.

increases from $\Theta = 1.41$ to about $\Theta = 1.45$. F and Θ change approximately linearly with $B_{\phi,\rm ext}(a)$.

4.2. Reduction of the dynamo electric field

As a next step, it was assumed that simultaneously with the change in $B_{\phi,\rm ext}(a)$ the dynamo electric field is decreased by a factor of 2, i.e. the parameter ξ is reduced from 1 to 0.5. This does not lead to any significant change in the time trace of the total input power with respect to the case of $j_{\rm ext}$ effect only, figure 4. It leads, however, to a remarkable change in the power density profile. In figure 6, $Q_{\rm OH}$ values at $t = 0.2$ and 1 ms are shown together with the reference profile at -2 ms. The power density profile peaks instantaneously and remains nearly constant for 5 ms, except at the very plasma edge, where $Q_{\rm OH}$ changes with the dissipation of $j_{\rm ext}$.

The total parallel current density, $j_{\parallel}^{\rm dyn+ext}$, and the poloidal and toroidal field profiles computed at the reference time, -2 ms, and at 0.2 and 1 ms are shown in figure 7. With the new field distribution, the reversal parameter, F, and the pinch parameter, Θ, change slightly compared with the results of 4.1: F deepens from -0.16 to -0.165 and Θ increases from 1.45 to 1.51. In the configuration with $\xi = 0.5$, the toroidal field is lower at the edge and higher in the centre (see figure 7(*c*)). Therefore the toroidal flux is decreased by 8% with respect to the pre-PPCD value. These results are in qualitative agreement with the experimental data [3, 24], although a single PPCD pulse modelled here differs from a train of PPDC pulses reported in [3].

The increase in the power density in the central plasma by more than 20% causes a relatively modest increase in the central electron temperature, from a pre-PPCD value of 212–225 eV (see figure 8). The temperature profile practically does not change during the PPCD stage. One could expect a more pronounced effect of the power density redistribution by considering the following non-linear feedback mechanism. An increase in the central power density leads to a higher temperature in the core, and the Lundquist number $S \sim T^{1.5}$ grows up. This causes a reduction in the magnetic fluctuation level, and accordingly, the transport coefficients are expected to decrease. This could lead to a further increase in the temperature and further reduction of transport.

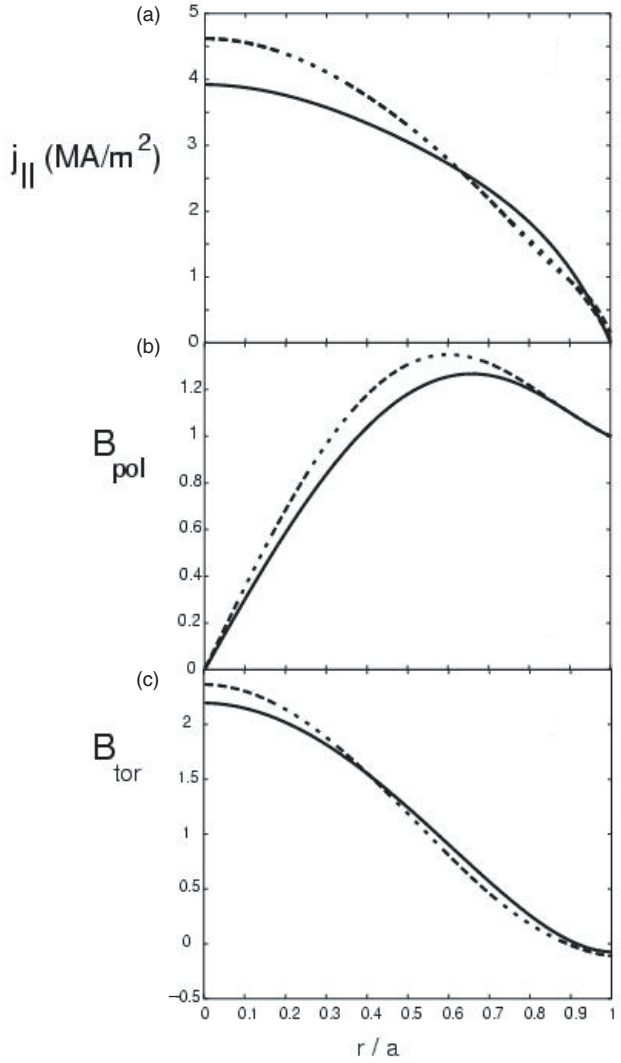

Figure 7. Radial profiles of the total parallel current (*a*) normalized poloidal field (*b*) and normalized toroidal field (*c*) calculated at the reference time, $t = -2$ ms (——), and at $t = 0.2$ and 1 ms. The profiles at $t = 1$ ms are indistinguishable from those at $t = 0.2$ ms.

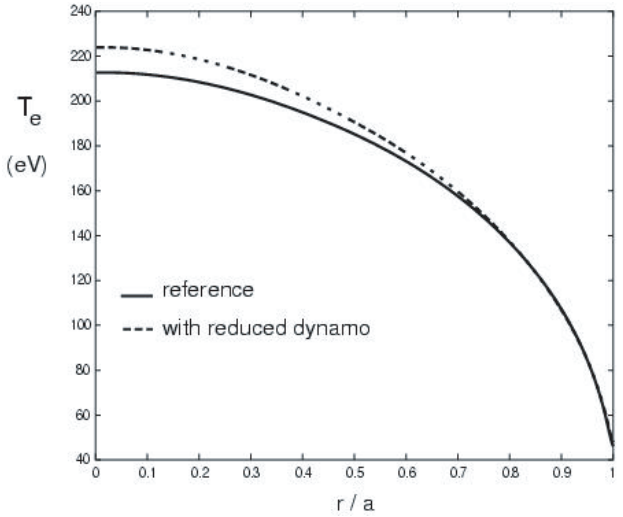

Figure 8. Electron temperature profile without and with the reduction in dynamo.

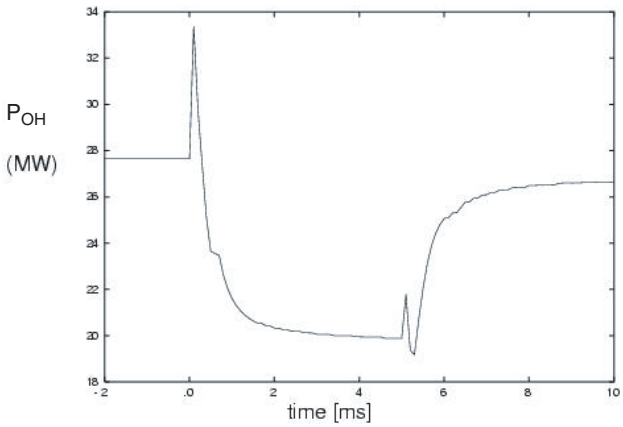

Figure 9. Time trace of the total power computed by taking into account the externally induced currents and the reduction in dynamo and magnetic fluctuations during the PPCD stage.

However, this effect is essentially compensated by the increase with temperature in the parallel heat conductivity, which governs the transport coefficients in a stochastic magnetic field (see equation (2)). Therefore, the results of our modelling allow us to conclude that the reduction in transport observed during PPCD cannot be caused only by the reduction in dynamo electric field and by the related central peaking of the power deposition profile.

4.3. Reduction of transport

Finally, in order to take into account the direct effect of PPCD on magnetic perturbations predicted by non-linear MHD simulations [7], the factor k in the dependence of $\delta b_r/B$ on the Lundquist number was reduced by 30%. Figure 9 shows the time evolution of the total input power in this case. One can see that after a transient phase of 1 ms the power decreases from the reference value of 27 MW to less than 20 MW. This happens because the increase in the electron temperature with reduced transport leads to a decrease in the plasma resistivity, $\eta \sim T_e^{-3/2}$. Radial profiles of the electron temperature computed at $t = -2$, 0.2, 0.4 and 2 ms when the temperature reaches its asymptotic form are shown in figure 10. The increase in the central T_e by about 90 eV during PPCD is in agreement with the data of Thomson scattering (see, e.g. figure 3 of [3]). The time evolution of the heating power density profile is shown in figure 11. At $t = 0.2$ ms, one can see only the effects from the dissipation of externally driven currents and from the reduction in the dynamo induced electric field. For the late time $t = 2$ ms, when the modifications in transport cause the increase in the central temperature, Q_{OH} becomes lower than in the pre-PPCD phase at all radii. The radial profiles of the electron heat diffusivity and effective particle diffusivity before ($t = -2$ ms) and during ($t = 2$ ms) PPCD are shown in figure 12.

It would be reasonable to expect that the reduction of transport under PPCD conditions should be of importance for the plasma density profile also. In RFX, under both standard and PPCD conditions, the electron density profile is

hollow at a sufficiently high density, $n_e > 4 \times 10^{19}\,m^{-3}$ [19]. The particle source due to recycling neutrals is weak in the main plasma and the balance between diffusive and convective components of the plasma flux governs the density profile. In the case without PPCD, the particle diffusivity is extremely large and the term proportional to the temperature gradient (see equation 3(*b*)) dominates the convective velocity. The latter is directed outwards, and the resulting density profile is hollow: $n_e \sim T_e^{-1/2}$. When the particle diffusivity is reduced during PPCD, the negative $E \times B$ contribution to the convection becomes more important and one would expect a transition to a peaked density profile. Such a transition, however, is not experimentally confirmed [3]. In order to ensure the hollowness of the density profile during the PPCD phase also the value of the inward $V_{E\times B}$ pinch-velocity had to be reduced in calculations by a factor of 2, from 7 m s^{-1} for the reference case to 4 m s^{-1} for PPCD. The physical mechanism responsible for the reduction in this transport channel should be identified in a future study (see also discussion in [7]).

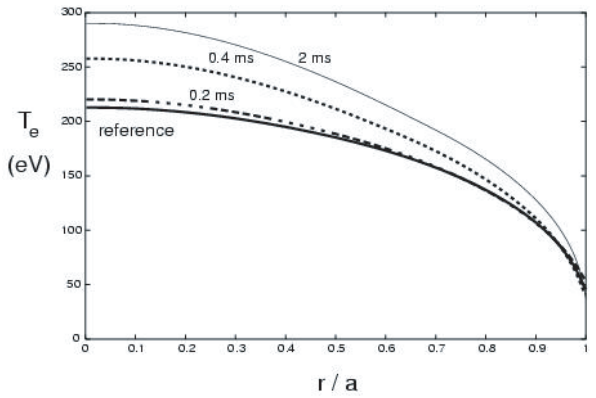

Figure 10. Electron temperature profile calculated at the reference time, $t = -2$ ms, and at $t = 0.2$, 0.4 and 2 ms. The effects of the external currents and of the reduction in the dynamo and fluctuation level are included.

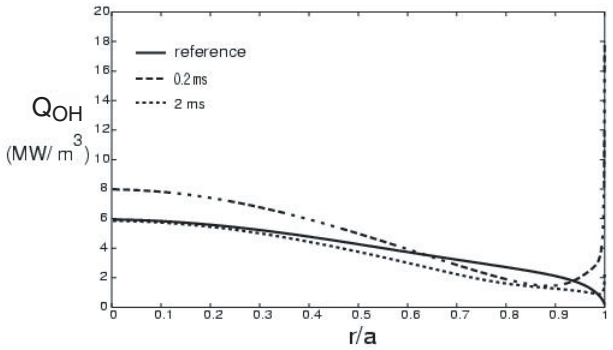

Figure 11. Power density profile at $t = -2$ ms (reference) and at $t = 0.2$ and 2 ms. The effects of the external currents and of the reduction in the dynamo and in the fluctuation level are included.

4.4. Modelling for trapezoidal form of PPCD pulse

As a more realistic approximation to the experimental time evolution of $B_{\phi,\mathrm{ext}}(a)$, we have considered a trapezoidal form, figure 1(*b*). The whole duration of the PPCD pulse, $2t_1 + t_2 = 5$ ms, was kept the same as for the step-like form, figure 1(*a*), and two cases with $t_1 = 0.4$ and 2 ms were modelled. The factors ξ and k, characterizing the reduction in the dynamo induced electric field and the decrease in magnetic perturbations, respectively, were assumed to change linearly with time during the intervals $0 \leqslant t \leqslant t_1$ and $t_1 + t_2 \leqslant t \leqslant 2t_1 + t_2$ from their value before PPCD to their top PPCD values and reverse, respectively.

Although the externally induced currents evolve differently compared with the case of the step function, no qualitative differences are seen in the behaviour of relevant magnetic parameters. For example, the parameters F and Θ reach after t_1 approximately the same values they reach instantaneously for the step function. The same can be said about the temperature and heating density profiles.

On the contrary, the transient jump in the total power at the beginning of PPCD, which is due to the dissipation of the externally driven currents, is very sensitive to the wave form

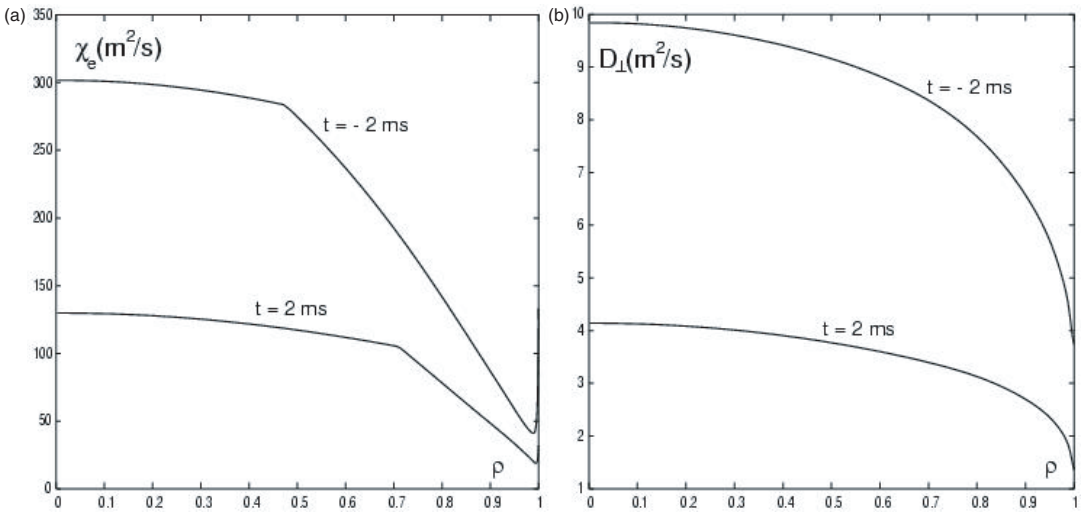

Figure 12. Radial profile of (*a*) the electron heat conductivity and (*b*) effective particle diffusivity at $t = -2$ ms and at $t = 2$ ms.

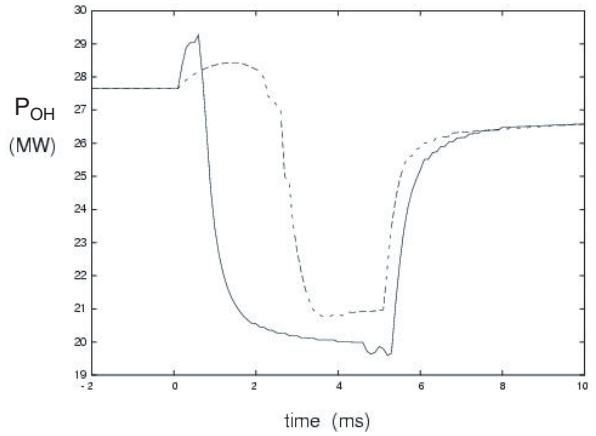

Figure 13. Time traces of the total power for trapezoidal time trace of $B_{\phi,\mathrm{ext}}$ computed with (*a*) $\Delta t_1 = 0.4$ ms (——) and (*b*) $\Delta t_1 = 2$ ms (- - - -). The power from j_{ext} as well as the effects of the reduction in the dynamo and the fluctuation level are included.

of $B_{\phi,\mathrm{ext}}(a)$. According to figure 13, this jump is reduced to a level of about 2 and 1 MW for $t_1 = 0.4$ and 2 ms, respectively, compared with 6–7 MW found for the instantaneous increase in $B_{\phi,\mathrm{ext}}(a)$ (see figures 4 and 9). These values have to be compared with the typical experimental value of 5 MW for the external power, P_{ext}, estimated from the current and voltage on the toroidal coils. It should be noted, however, that in the case of the trapezoidal waveform the computed transient increase in the total power, P_{OH}, shortly after $t = 0$ (see figure 13) is smaller than the actual power generated by j_{ext}. This is due to the fact that since P_{OH} is calculated including all the currents in the plasma, the power generated by j_{ext} is partly compensated by the simultaneous decrease in the fluctuation level in the central plasma and hence of the loop voltage. At a later stage of PPCD, for $3 \leqslant t \leqslant 5$ ms, all computational scenarios give a reduction of the total power of about 25% of the reference value (see figures 9 and 13). This is in good agreement with a typical decrease in the loop voltage of 30% observed during PPCD [3].

To conclude, note that normally P_{ext} is not included into the power balance and therefore the transient increase in P_{OH} at the beginning of PPCD is not seen in experimental traces, as in [3]. Thus, the computed total power, P_{OH}, may be compared with the experimental values of the loop voltage only at times when the contribution from externally driven currents is already very low, i.e. in our case for $t > 2$ ms.

5. Discussion and conclusions

The one-dimensional transport code RITM applied earlier for modelling of standard discharges in RFX was developed further in order to simulate the modification of plasma profiles under conditions of PPCD. The amendments done in the code allow us to take into account (i) the evolution of externally induced electric currents, (ii) the reduction in dynamo and (iii) decrease in magnetic field fluctuations. The level of changes in dynamo induced electric field and radial component of magnetic fluctuations was taken from the results of non-linear MHD simulations and from experimental data. The computations were performed by including step by step all the above-mentioned channels. It is found that externally driven currents are resistively dissipated at the plasma edge and lead to a transient increase in Ohmic input power. This power contribution is, however, lost very fast from the plasma and leads neither to any increase in the temperature nor to peaking of the current profile. The reduction in dynamo electric field with PPCD leads to a redistribution of the power deposition profile, so that it becomes more centrally peaked. By including this mechanism in RITM, it was possible to get the peaking of the power and current density profiles, while the level of the total power remains practically unchanged and the central temperature increases very moderately. Thus, these results demonstrate that both the presence of externally driven currents and the reduction in the dynamo field cannot explain the measured increase in the central temperature. On the other hand, it is possible to reproduce in simulations a significant rise in the central temperature (of the order of 90 eV) by reducing the level of the amplitude of magnetic perturbations by 30%, as was identified in non-linear MHD simulations. With decreased δb_{r}, the effective heat conductivity due to transport along stochastic magnetic field lines is reduced by a factor of 2–2.5. The total heating power decreases from 27 to 20 MW, in good agreement with a 30% reduction in the experimentally measured loop voltage.

In order to achieve full self-consistency, transport simulations should be coupled with non-linear MHD modelling. This might be of particular importance for the evolution of externally driven currents. Indeed, recent MHD results [7] show that, in addition to the resistive diffusion, a strong turbulent convection can essentially contribute to the radial transport of these currents. In this case, they can penetrate deeper into the plasma core and lead to a stronger modification of equilibrium currents. This would mean that the role of external currents in the plasma core is likely underestimated in the present modelling. In addition, it should be emphasized again that the results of this paper were obtained under the assumption $E_{\mathrm{i}\varphi}(r) = \mathrm{const}$, which is violated for transient processes with a characteristic time of 1 ms. Therefore, the computed level of the spike in the Ohmic power in the early phase of PPCD, as it appears in figures 4 and 9, has to be considered simply as a qualitative result. A future development of the modelling approach should definitely take into account the radial variation of $E_{\mathrm{i}\varphi}(r)$.

Acknowledgments

It is a pleasure to thank S. Ortolani for carefully reading and commenting on the manuscript. Helpful discussions with R. Lorenzini, R. Paccagnella and M.E. Puiatti are also kindly acknowledged. Special thanks are due to S. Cappello for comments and suggestions. Constructive comments from the referees are gratefully acknowledged.

Appendix A. Magnetic field consistent with the current density, $j_{\parallel}^{\mathbf{dyn}}$

The Maxwell equation for a force-free configuration, $\vec{\nabla} \times \vec{B} = (4\pi/c)\vec{j} = \mu\vec{B}$, can be rewritten in the following system of equations for the components of the normalized field $\vec{b} = \vec{B}/B_\theta(a)$

$$\frac{\mathrm{d}b_\varphi}{\mathrm{d}\rho} = -\frac{w}{b}b_\theta, \qquad \frac{\mathrm{d}b_\theta}{\mathrm{d}\rho} + \frac{b_\theta}{\rho} = \frac{w}{b}b_\varphi,$$

where the parameter $w = (4\pi/c)(a/B_\theta(a))j_\parallel^{\rm dyn}$ is fixed. After some algebra, one can obtain the equations for $b^2 = b_\theta^2 + b_\varphi^2$ and $\psi = \rho(b_\varphi/b_\theta)$

$$\frac{{\rm d}b^2}{{\rm d}\rho} = -\frac{2\rho}{\rho^2+\psi^2}b^2,$$
$$\frac{{\rm d}\psi}{{\rm d}\rho} = \frac{1}{\rho}\left[2\psi - \frac{w}{b}(\rho^2+\psi^2)\right],$$

with boundary conditions

$$b^2(1) = 1 + \psi^2(1) \qquad \text{and} \qquad \psi(0) = \frac{2b(0)}{w(0)}.$$

These equations are integrated numerically by iterations starting with the equilibrium pre-PPCD profile for $b(\rho)$. First, the boundary value, $\psi(0)$, is determined and the equation for $\psi(\rho)$ is integrated. With known $\psi(1)$, one determines the boundary value, $b^2(1)$, and integrates the equation for b^2. This procedure is repeated till the required accuracy is reached.

Appendix B. Total parallel current density

In the presence of an externally induced toroidal field and poloidal current, the total current density, $j_\parallel^{\rm ext+dyn}$, is determined as

$$j_\parallel^{\rm ext+dyn} = \frac{(\vec{b}+\vec{b}_{\rm ext})\cdot(\vec{j}^{\rm dyn}+\vec{j}_{\rm ext})}{|\vec{b}+\vec{b}_{\rm ext}|},$$

where $\vec{b}_{\rm ext} = (B_{\varphi,{\rm ext}}/B_\theta(a)) \times \vec{e}_\varphi$ and $\vec{j}_{\rm ext} = j_{\rm ext}\vec{e}_\theta$. This leads to

$$j_\parallel^{\rm ext+dyn} = \frac{(b + (b_{\rm ext}b_\varphi/b))j_\parallel^{\rm dyn} + j_{\rm ext}b_\theta}{\sqrt{b_\theta^2 + (b_\varphi + b_{\rm ext})^2}}.$$

References

[1] Sarff J.S. *et al* 1995 *Phys. Plasmas* **2** 2440
[2] Rostagni G. 1995 *Fusion Eng. Des.* **25** 301
[3] Bartiromo B. *et al* 1999 *Phys. Rev. Lett.* **82** 1462
[4] Sovinec C.R. and Prager S.C. 1999 *Nucl. Fusion* **39** 777
[5] Ortolani S. and Schnack D.D. 1993 *Magnetohydrodynamics of Plasma Relaxation* (Singapore: World Scientific)
[6] Cappello S. and Biskamp D. 1996 *Nucl. Fusion* **36** 571
[7] Puiatti M.E. *et al* 2003 *Nucl. Fusion* **43** 1057
[8] Tokar M.Z. 1994 *Plasma Phys. Control. Fusion* **36** 1819
[9] Tokar M.Z. *et al* 1997 *J. Nucl. Mater.* **241–243** 528
[10] Carraro L. *et al* 2000 *Nucl. Fusion* **40** 1983
[11] Telesca G. and Tokar' M.Z. 2000 Simulation of RFX plasmas by the self-consistent code RITM *27th EPS Conf. on Controlled Fusion and Plasma Physics (Budapest, 12–16 June 2000)* vol 24B (ECA) pp 308–11
[12] Rosenbluth M.N. *et al* 1966 *Nucl. Fusion* **6** 297
[13] D'Angelo F. and Paccagnella R. 1996 *Phys. Plasmas* **3** 2353
[14] Terranova D. *et al* 2000 *Plasma Phys. Control. Fusion* **42** 843
[15] Intravaia A. *et al* 1999 *Phys. Rev. Lett.* **83** 5499
[16] Rechester A.B. and Rosenbluth M.N. 1978 *Phys. Rev. Lett.* **40** 38
[17] D'Angelo F. and Paccagnella R. 1999 *Plasma Phys. Control. Fusion* **41** 941
[18] Capes H. *et al* 1992 *Contrib. Plasma Phys.* **32** 192
[19] Gregoratto D. *et al* 1998 *Nucl. Fusion* **38** 1199
[20] Harvey R.W. *et al* 1981 *Phys. Rev. Lett.* **47** 102
[21] Tokar M.Z. 1999 *Phys. Plasmas* **6** 2808
[22] Carraro L. *et al* 2002 *Plasma Phys. Control. Fusion* **44** 2135
[23] Ortolani S. 1985 Stationary reversed field pinch profiles *Twenty Years of Plasma Physics* ed B. McNamara (Singapore: World Scientific) pp 75–94
[24] Bolzonella T. *et al* 1997 Magnetic profiles behaviour, dynamo mechanisms and confinement in RFX *24th EPS Conf. on Controlled Fusion and Plasma Physics* (*Berchtesgaden, Germany, 9–13 June 1997*) vol 21A (part I) pp 317–20